



Scale-up agitation criteria for *Trichoderma reesei* fermentation

Nicolas Hardy, Frédéric Augier, Alvin W. Nienow, Catherine Béal, Fadhel Ben Chaabane

► To cite this version:

Nicolas Hardy, Frédéric Augier, Alvin W. Nienow, Catherine Béal, Fadhel Ben Chaabane. Scale-up agitation criteria for *Trichoderma reesei* fermentation. *Chemical Engineering Science*, 2017, 172, pp.158-168. 10.1016/j.ces.2017.06.034 . hal-01544606

HAL Id: hal-01544606

<https://agroparistech.hal.science/hal-01544606>

Submitted on 9 Mar 2018

HAL is a multi-disciplinary open access archive for the deposit and dissemination of scientific research documents, whether they are published or not. The documents may come from teaching and research institutions in France or abroad, or from public or private research centers.

L'archive ouverte pluridisciplinaire **HAL**, est destinée au dépôt et à la diffusion de documents scientifiques de niveau recherche, publiés ou non, émanant des établissements d'enseignement et de recherche français ou étrangers, des laboratoires publics ou privés.



Distributed under a Creative Commons Attribution - ShareAlike 4.0 International License

Scale-up agitation criteria for *Trichoderma reesei* fermentation

Nicolas Hardy¹⁻²⁻³, Frédéric Augier², Alvin W. Nienow⁴, Catherine Béal³, Fadhel Ben Chaabane¹

¹IFP Energies nouvelles, 1 et 4 avenue de Bois-Préau, 92852 Rueil-Malmaison, France

²IFP Energies nouvelles, Rond-point de l'échangeur de Solaize, BP3, 69360 Solaize, France

³UMR 782, AgroParisTech INRA, 1 avenue Lucien Brétignières, 78850 Thiverval-Grignon, France

⁴School of Chemical Engineering University of Birmingham, Edgbaston, Birmingham B15 2TT, United Kingdom

Contact details: Corresponding author is Frederic Augier, +33 4 37 70 21 42, e-mail:

frederic.augier@ifpen.fr

ABSTRACT

Scale-up of aerobic fungal fermentation processes still remains a challenging issue for the biotechnology industry. This difficulty arises due to the complex interactions between operating conditions (agitation, aeration, etc.), the physicochemical state of the broth (viscosity, the dissolved oxygen concentration, etc.) and the biology of fungi (growth, production, morphology, etc.). Because of their size, filamentous fungi are affected by fluid dynamic stresses but quantification of this complex parameter is a difficult task. In general, indirect criteria are used for the effect of fluid dynamic stresses on scale-up (tip speed, power draw or the energy dissipation/circulation function (EDCF)). In order to better understand the impact of such criteria on the fermentation of the fungus *Trichoderma reesei*, a wide range of agitation conditions has been explored. The morphology of *T. reesei* fungus, its specific growth rate and the rheological properties of the broth have all been measured both at bench

scale (~ 2.5 L) and for the first time, at a typical commercial scale. These three aspects of the fermentation at both scales were then compared with respect to tip speed, specific power and EDCF. This work has shown that tip speed as a correlator of any of these parameters is totally ineffective whilst the EDCF is clearly the best for extrapolating laboratory data to the commercial scale.

KEYWORDS

Trichoderma reesei, scale-down, scale-up, morphology, rheology, filamentous fungus.

1. INTRODUCTION

Biofuels are candidates to substitute oil with a lower carbon footprint. Among them, bioethanol is the most consumed biofuel in the world (Simbolotti 2007) and bioethanol from lignocellulosic resources (also called second generation bioethanol) appears to be a good candidate to reduce CO₂ production (Percival Zhang et al. 2006). The biotransformation of lignocellulosic biomass involves the utilization of specific enzymes named cellulases (Bischof et al. 2016), which are needed to degrade cellulose into simple and fermentable sugars. However, the cost of these enzymes is one of the limiting factors of bioethanol production from cellulolytic materials. To decrease the impact of the cost of cellulase on the price of ethanol, different advances can be targeted. Firstly, the efficiency of the enzymatic cocktail has to be improved in order to reduce the amount of enzymes needed during the hydrolysis (Ayrinhac et al. 2011). Secondly, the production capacity has to be developed by means of an efficient process optimization and scale-up strategy (Percival Zhang et al. 2006). Nowadays, cellulase production is mainly performed with the filamentous fungus *Trichoderma reesei* (Gusakov 2011). This microorganism is known for its high cellulase

secretion capacity and productivity (Gusakov 2011). An efficient protocol for cellulase production (Pourquié et al, 1988) consists of two sequential phases: a batch phase followed by a fed-batch phase. The fungus first grows during the batch phase, with sugar and nutrients in excess, in order to produce a large concentration of cellular biomass. During this step, the enzyme production keeps low and nutrients are mainly used for the growth of the fungi. The latter has a hyphal structure exhibiting a highly viscous, non-Newtonian behaviour. In the subsequent fed-batch phase, a limiting rate of sugar is fed continuously to the bioreactor to favor the synthesis of the enzyme. During this phase, the hyphae break down and the viscosity falls. At the same time, the oxygen requirement by microorganisms is also strongly decreased. Thus, the most challenging phase with respect to the specific energy input required for effective agitation is the first, as it requires the highest oxygen transfer rate during the period of highest viscosity (Gabelle et al. 2012).

Furthermore, despite their high productivity, *T. reesei* fermentations are difficult to scale-up due to the complex rheology of the broth during the biomass growth phase. The hyphal development induces an increase of the broth viscosity with a shear thinning behaviour (Gabelle et al. 2012; Hardy et al. 2015; Malouf et al. 2013). The shear thinning behaviour induces changes in the hydrodynamics of the broth that tend to increase spatial heterogeneities and may lead to caverns formation in the bioreactor (Amanullah et al. 2002; Marten et al. 1996; Stocks 2013). In addition, *T. reesei* is strictly aerobic and the increase of viscosity also strongly reduces the rate of oxygen mass transfer (Gabelle et al. 2012). To ensure a sufficiently high rate, the power input has to be increased, which results in an increase of the fluid dynamic stresses on the mycelial structures, which because of their size and filamentous nature are prone to size reduction (Serrano-Carreón et al. 2015). Thus, the fungus morphology impacts process parameters and the process conditions affect in return the

fungus morphology. Though significant advances in understanding these interrelations have been made in the past (Amanullah et al. 2002; Jüsten et al. 1996), their impact on processes at the full industrial scale is still not fully understood, especially because the magnitude of the fluid dynamic stresses changes with scale (Stocks 2013). All those elements show that the scale-up of the process is complex and that these changes in fluid dynamic conditions have to be included in order to scale-up process involving filamentous fungus such as *T. reesei*. The fluid dynamic stress that affects the microorganism morphology and possibly its productivity in a bioreactor have often been called ‘shear stress’ (or just ‘shear’), but the precise nature of the stress that causes such damage is not known in the complex three dimensional turbulent or near turbulent flow field found in bioreactors with a very wide range of local specific energy dissipation rates. Therefore, the term will not be used here. Whatever the mechanism that damages microorganisms, it has generally been related to relatively simple and quantifiable parameters, namely the impeller tip speed, the specific power input into the bioreactor by the impeller (or mean specific energy dissipation rate), or to the concept of an “energy dissipation/circulation” function, EDCF (Gabelle et al. 2012; Jüsten et al. 1996; Sánchez Pérez et al. 2006). Indeed, it was suggested many years ago that the tip speed of the impeller (V_{tip}) was a measure of the ‘maximum stress’ (Oldshue 1966). V_{tip} is given by Eq.1:

$$V_{tip} = \pi \times D \times N \quad (1)$$

where D is the diameter of the impeller (m) and N the rotational speed (s^{-1}). This concept appears to have received wide acceptance in the biochemical engineering community (Bailey and Ollis 1986; Wang et al. 1979), though there seems to be little experimental evidence to support it. Another approach is to use an estimate based on an average shear rate but this is dependent on the flow regime. In the laminar flow regime, the Metzner-Otto approach

(Metzner and Otto, 1957) can be used. However, even at the bench scale, the Reynolds number (Re) $\gg 10$, thus much higher than that which defines laminar flow. In the turbulent regime, the average shear rate can be linked to the mean specific energy dissipation rate and kinematic viscosity for a Newtonian fluid. The power draw per unit of volume (P/V , $W.m^{-3}$) is equivalent to the mean specific energy dissipation rate (Sánchez Pérez et al. 2006) where power P can be determined from Eq. 2 (Stocks 2013):

$$P = Po \times \rho \times N^3 \times D^5 \quad (2)$$

where Po is the power number of the impeller (dimensionless) and ρ the density of the broth ($kg.m^{-3}$). Though here, at the bench scale, the flow is transitional ($Re < 2 \times 10^4$) and the fluid is non-Newtonian (shear thinning), it is certainly closer to turbulent flow than laminar, at least in the impeller region, where energy is mostly dissipated. As an approach based on the transitional regime is not available, turbulent flow relationships are generally assumed. A more sophisticated approach uses the “energy dissipation/circulation” function EDCF where again the assumption of turbulent flow is made. It was first proposed by Smith et al. (1990); here the potential for damage was related to the energy dissipated in the region of a Rushton turbine impeller and the frequency of the passage of the mycelium through that region. This basic concept was modified by Jüsten et al. (1996) to include an additional geometrical factor (k) by which the relevant volume depended on impeller type and a volume swept out by it as it rotated. In this way, different kinds of impeller could be compared. Thus Eq.3:

$$EDCF = \left(\frac{P}{k \times D^3} \right) \left(\frac{1}{t_c} \right) \quad (3)$$

Here EDCF is in $\text{W.m}^{-3}.\text{s}^{-1}$, k is a dimensionless constant and t_c the circulation time (s) that is obtained from Eq.4:

$$t_c \approx \frac{V}{Fl \times N \times D^3} \quad (4)$$

where V is the liquid volume in the bioreactor (m^3) and Fl is the Flow number of the impeller (dimensionless). The power draw in the swept volume is used in Eq.3 to represent the energy ‘perceived’ by the fungus during its passage through the impeller. This concept relies on the Kolmogorov’s theory of isotropic turbulence that connects dissipation rate and shear rate or stress (Kolmogorov, 1941). Jüsten et al. (1996) showed that the EDCF concept can be correlated to the size reduction of the mycelia due to agitation with a wide range of impellers at bench and small pilot plant scale with *P. chrysogenum*; and Amanullah et al. (2000) showed its applicability to *A. oryzae*. Nevertheless, there are issues to be resolved such as how to determine the value of the parameter k for complex impellers. As an alternative to the determination of appropriate k values, it is proposed in the present study to use the maximum specific energy dissipation rate (ϵ_{\max}) in W/m^3 , instead of P/kD^3 , which leads to the definition of the new criteria, $\text{EDCF}_{\epsilon_{\max}}$:

$$\text{EDCF}_{\epsilon_{\max}} = \frac{\epsilon_{\max}}{t_c} \quad (5)$$

Though the maximum local specific energy dissipation rate (ϵ_{\max}) is difficult to determine experimentally since laser based techniques such as PIV or LDA followed by complex data manipulation must be used (Gabriele et al. 2009), it has been shown by Grenville and Brown (2012) that it can be estimated from Eq.6:

$$\varepsilon_{max} = 1.04 \times \rho \times P o^{\frac{3}{4}} \times N^3 \times D^2 \quad (6)$$

149

150 There are also some other related studies in the literature. For example, Malouf et al. (2013)
 151 explored the relationships between *T. reesei* morphology, rheology and biomass
 152 concentration as a function of rotational speed. Other studies are focused on the impact of
 153 agitation intensity and agitation devices on cellulase production (Marten et al. 1996; Patel et
 154 al. 2009). However, to our knowledge, no work has been reported with such data for *T. reesei*
 155 cultures from the laboratory scale to the industrial scale. In addition, as Quintanilla et
 156 al. (2015) underlined, most of published studies on filamentous fermentation were made
 157 under conditions that are quite different from industrial ones (low-producing strains, growth
 158 with substrate and/or oxygen limitations, utilization of pure substrates, not optimized
 159 processes, etc.).

160 The goal of this work is to identify scientifically based scale-up criteria for filamentous fungi
 161 fermentations. To do so, the three representations of fluid dynamic stress discussed above
 162 will be determined for a wide range of *T. reesei* fermentation conditions at laboratory scale.

163 The ability of these criteria to correlate with growth rate, fungal morphology and rheology is
 164 discussed.

165 As, uniquely, some data are available from commercial scale, the three candidates as “stress”
 166 criteria are also determined for the large scale conditions as a test of robustness for scale-up
 167 considerations.

168 2. MATERIALS, METHODS AND EXPERIMENTAL PREREQUISITES

169 *Fungus strain*

170 The industrial strain of *Trichoderma reesei* Tr3002 (IFPEN culture collection) was used. It
 171 derived from the strain *T. reesei* CL847 obtained by classical and molecular genetics (Durand

et al. 1988). It displayed an improved β -glucosidase gene, a hyperproducing cellulases capacity and was glucose-derepressed (Ayrinhac et al. 2011). Conservation was made in spores form at a concentration of 2×10^7 colony forming units per milliliter. Spores were stored on frozen form in water added with 50 % glycerol, at -80°C .

Culture media

The preculture medium was composed of di-potassium phthalate 0.02 mol.L^{-1} ; (Na_2MoO_4 , $2 \text{ H}_2\text{O}$) 1.25 mg.L^{-1} ; (CuSO_4 , $5 \text{ H}_2\text{O}$) 2.4 mg.L^{-1} ; (MnSO_4 , H_2O) 5.12 mg.L^{-1} ; (ZnSO_4 , $7 \text{ H}_2\text{O}$) 6.72 mg.L^{-1} ; ($\text{Co}(\text{NO}_3)_2$, $6 \text{ H}_2\text{O}$) 7.2 mg.L^{-1} ; (FeSO_4 , $7 \text{ H}_2\text{O}$) 24 mg.L^{-1} ; (Na_2HPO_4 , $12 \text{ H}_2\text{O}$) 92 mg.L^{-1} ; (CaCl_2 , $2 \text{ H}_2\text{O}$) 0.48 g.L^{-1} ; (MgSO_4 , $7 \text{ H}_2\text{O}$) 0.48 g.L^{-1} ; (NH_4) $_2\text{SO}_4$ 2.24 g.L^{-1} ; H_3PO_4 85% 2.4 mL.L^{-1} ; KOH 1.33 g.L^{-1} and corn steep solid 2 g.L^{-1} . pH was adjusted to 5.25 with NaOH 7 mol.L^{-1} .

For bioreactor cultivation, the culture medium included (Na_2MoO_4 , $2 \text{ H}_2\text{O}$) 1 mg.L^{-1} ; (CuSO_4 , $5 \text{ H}_2\text{O}$) 3.0 mg.L^{-1} ; (ZnSO_4 , $7 \text{ H}_2\text{O}$) 8.4 mg.L^{-1} ; (MnSO_4 , H_2O) 6.4 mg.L^{-1} ; ($\text{Co}(\text{NO}_3)_2$, $6 \text{ H}_2\text{O}$) 9 mg.L^{-1} ; (FeSO_4 , $7 \text{ H}_2\text{O}$) 30 mg.L^{-1} ; (Na_2HPO_4 , $12 \text{ H}_2\text{O}$) 115 mg.L^{-1} ; (CaCl_2 , $2 \text{ H}_2\text{O}$) 0.6 g.L^{-1} ; (NH_4) $_2\text{SO}_4$ 2.8 g.L^{-1} ; H_3PO_4 85% 3 mL.L^{-1} ; KOH 1.66 g.L^{-1} ; corn steep solid 2 g.L^{-1} . Antifoam SB2121 from Strucktol (Hamburg, Deutschland) was added at 1 % (v/v) and pH was adjusted with NH_3 10.25 % (v/v) to 4.8.

All media were sterilized by autoclaving at 121°C for 20 min.

Precultures

A volume of 250 mL of preculture medium was prepared in a 2 L Fernbach flask by mixing 225 mL of preculture medium and 25 mL of a sterile glucose solution at 250 g.L^{-1} . The flasks were seeded with 1 mL of thawed spores and incubated in a shaker Multitron II (Infors, Bottmingen, Switzerland) at 30°C for 70 h. The agitation was set to 180 rpm with an orbital of 50 mm.

Cultivation at bench scale

The preculture was used to inoculate a 3.5 L bioreactor (IFPEN, Rueil-Malmaison, France) containing 2.5 L culture medium (1.75 L of culture medium and 500 mL of sterile industrial grade glucose solution at 250 g.L⁻¹) as previously described by Gabelle et al.(2012). Fermentations were performed in batch culture mode and each was repeated once (run in duplicate). Temperature was set at 27°C, pH was maintained at 4.8 with NH₃ (10.25 %, v/v) and gas flow rate was fixed at 1.25 L.min⁻¹ (0.5 VVM). Agitation was carried out by using four different kinds of impeller (Fig. 1) that were characterized by their shape, their dimensions, their number of blades, their power number and their flow number (Table 1). Power and flow numbers were provided by the suppliers, except for the four-blade disk paddle one, which was determined by CFD simulation. They were driven by an asynchronous electric motor 1LA7063 4AB12 (Siemens, Munich, Germany) controlled by a variable speed drive ATV31C018M2 (Schneider, Rueil-Malmaison, France) at four different stirring rates: 800 min⁻¹, 935 min⁻¹, 1250 min⁻¹ and 1700 min⁻¹. Dissolved oxygen (dO₂) concentration was measured with an InPro 6860i optical oxygen sensor (Mettler-Toledo, Greifensee, Switzerland) and controlled by the admission of a gas mix composed of nitrogen and compressed air. The gas mix was achieved by two gas flow mass controllers EL-FLOW F-201CV (Bronkhorst, Ruurlo, The Netherlands) that permitted the bioreactor gas flow rate to be kept constant. dO₂ was set at 40 %, to be higher than the critical dissolved oxygen concentration of ~15% at atmospheric pressure (Marten et al. 1996) so that the culture performance should be independent of oxygen concentration. The constraint on the minimal dissolved oxygen set a minimal P/V of 6 kW.m⁻³ below which the minimal value of 40% is not reached. The minimal stirring rate of 800 RPM was able to meet this requirement for the four tested impellers.

Seven fermentation experiments were used in the present study. All cultivation have been duplicated. Fermentations were stopped before the end of the exponential growth phase, with residual glucose concentration above than 1 g.L^{-1} . Samples were collected at least twice every 24 h for biomass and glucose concentration analyses. Rheological property measurements and image analyses were made on samples collected with a biomass concentration between 4 and 8 g. kg^{-1} .

Cultivation at industrial scale

Uniquely, two experiments were conducted at a commercial scale with the same strain. One was a full run in which growth rate, morphology and rheology were measured in exactly the same way as at the bench scale. In an additional preliminary run, the growth rate was measured in the same way but the rheology was measured at a slightly higher biomass concentration before the method had been standardised. At that time, the new image analysis technique had not been established. However, at this scale, there was no possibility of duplicating the one full experiment because of the cost and time involved.

With respect to the bioreactor configuration, for reasons of commercial confidentiality, only those aspects critical to the application of the three estimates of fluid dynamic stress can be given. Similar operating conditions with respect to dO_2 , temperature and gas flow rate were used. The total volume of the bioreactor was 220 m^3 and the liquid volume was between 80 and 130 m^3 . As usual at these scales, the vessel was equipped with multiple impellers, in this case one high power number impeller at the bottom and several down-pumping hydrofoil impellers of much lower power number above, each of the same diameter. The operating conditions at industrial scales are constrained first by the performances of the existing stirring device, which delivers a rather low specific power consumption compared to bench scale bioreactors. But as similar VVM was applied at both scales to avoid any inhibition by the dissolved CO_2 , the gas linear velocity is much higher at industrial scale, which enhances k_La

(van' t Riet and Tramper, 1991). At the same time, the static pressure also increases the average dissolved oxygen concentration at large scale and the Reynolds number is higher (Stocks, 2013). Consequently, the oxygen transfer rate is enhanced so that the specific power requirement (P/V) was about 10 times lower than at bench scale for a similar oxygen uptake rate.

Interestingly, in some preliminary lab-scale experiments operated with a specific power of $\sim 1 \text{ kW/m}^3$ (the same specific power as at the industrial scale) satisfactory fermentations could not be conducted due to dO_2 being too low, as also reported by Amanullah et al. (2002) with *Aspergillus oryzae*. In addition, the biomass grew as one large pellet of fungi of completely different morphology. On the other hand, the agitation conditions at the bench scale required to give the desired dO_2 at obtainable sparge rates led to a minimum tip speed of the impellers of 3.7 m.s^{-1} at the bench scale, which matched approximately the tip speeds used at the commercial scale.

The common use of multiple impellers at the commercial scale whilst typically only one is used at bench scale generally poses specific problems for scale up as geometric similarity is not maintained. Clearly if tip speed is being assessed, then since this parameter is independent of the number of impellers, a direct comparison can be made as the impellers are of the same size. If specific power, P/V , is under consideration, though the high power number impeller clearly inputs more power, for the impeller spacing used here, the total power can be evaluated by summing the power numbers (Nienow 1998) and using Eq.2. Finally, for assessment of $EDCF_{\epsilon_{\max}}$, as the Po ratio of the high Po impeller to the low one was > 3 , the ϵ_{\max} value is clearly much higher for the high Po impeller. Therefore, it should be used for estimating the appropriate $EDCF_{\epsilon_{\max}}$ value.

In addition, in order to estimate $EDCF_{\epsilon_{\max}}$ at the commercial scale, there is also a problem in estimating the circulation time, t_c for multiple impellers. At the bench scale, the flow number

of a single impeller is used to estimate it via the simple concept implied by Eq.4. Here, it was decided to evaluate t_c from the mixing time, t_m using the long standing equation, Eq.7 (van't Riet and Tramper 1991).

$$t_m = 4 \times t_c \quad (7)$$

Therefore, the mixing time was measured by a pulse injection of 5 liters of a solution of ammonia (25 % w/w) at the top of the bioreactor and the measurement of the pH at the bottom (Singh et al., 1986). The time response of the pH probe was below 5 s and the method was found to be robust with measurements being repeatable within approximately ± 3 s. Thus, $EDCF_{\epsilon_{\max}}$ could be determined from Eq.6 and Eq.7.

In order to have confidence in the mixing time measurements, they have been compared to a correlation available for multiple impeller configurations. Cooke et al. (1988) developed an initial correlation for multiple radial flow impeller configurations (Rushton turbines). These authors observed that in case of combination of radial and axial flow impellers, the mixing times are reduced by a factor ~ 2 at the same mean specific energy dissipation rate. As recommended by Nienow (1998), the correlation of Cooke et al. (1988) has been modified to allow for this reduction and in that case, the values predicted are very close (within 10%) to the present mixing time measurements. This consistency strengthens the use of the measured mixing times to calculate $EDCF_{\epsilon_{\max}}$.

Rheological property measurements

It is well known that with increasing biomass concentration, the apparent viscosity increases. For a given fungi, whilst this increase is dominated by biomass concentration, it has been shown that it also depends on the size of the filamentous entities or clumps, the larger the

clumps the higher the apparent viscosity at a particular shear rate due to increasing entanglement between clumps (Riley et al. 2000, Wucherpfennig et al. 2010). In order to minimize the link between biomass and apparent viscosity, rheological property measurements were made on samples taken during the exponential growth phase with a biomass concentration between 4 and 8 g/kg so that difference between fermentations was very predominantly associated with changes in clump size due to different agitation conditions as all other parameters (initial media composition, pH, temperature, dO₂, etc.) were held constant.

A rotational rheometer AR2000 (TA Instruments, New Castle, Delaware, the United States) equipped with a helical rotor, was used to carry out rheological property measurements (Hardy et al. 2015) at 27°C under controlled shear rates of 1 to 100 s⁻¹. Two cycles were performed during which shear rate was increased (from 1 to 100 s⁻¹) and decreased (from 100 to 1 s⁻¹) in 20 steps. Measurements of dynamic viscosity (η_a , Pa.s) were recorded when a steady state was achieved, i. e. when 3 consecutive values with less than 5 % variation were reached at each step. Results were considered with this method to have an uncertainty of 5% associated with the Couette analogy (Hardy et al. 2015).

In order to exclude possible errors due to secondary flow effects (Mezger 2014), only measurements with Taylor numbers < 1700 and Reynolds numbers < 53 were retained. Then, the Hershel-Bulkley (HB) model (Mezger 2014) was used to fit the rheograms and hence the fermentation broth apparent viscosity (Eq.8).

$$\eta_a = \frac{\tau_{HB}}{\dot{\gamma}} + K_{HB} \times \dot{\gamma}^{n-1} \quad (8)$$

with η_a the dynamic apparent viscosity (Pa.s), τ_{HB} the yield stress (Pa), $\dot{\gamma}$ the shear rate (s⁻¹), K_{HB} the consistency index (Pa.sⁿ), and n the flow behaviour index. The parameter τ_{HB} was

used to estimate the potential cavern diameter relative to the diameter of the tank (Elson et al. 1986). For all experiments, the predicted diameter of the cavern was greater than the diameter of the tank, so that no cavern formation issues were expected (Stocks 2013).

For comparing quantitatively the impact of agitation intensity associated with each impeller type and agitator speed on broth apparent viscosity, in each case the latter were determined at a reference shear rate of 10 s^{-1} . This shear rate is not the average shear rate present in the bioreactors, that indeed varies between geometries and stirring rates. But as set out above, it allows a simple and factual criteria for rheological property/apparent viscosity comparisons as measure of the impact of agitation on structure of the filamentous mycelia at the different scales.

Biomass concentration determination

The dry weight method was used to quantify the biomass concentration. A weighed glass microfiber filter (Whatman GF/C filters) was used to filter a weighed sample of the culture broth with particle retention of $1.2 \text{ }\mu\text{m}$. One volume of the sample was washed with three volumes of distilled water and oven-dried at 105°C until constant weight. The sample was weighted after cooling in a desiccator to reach room temperature, thus allowing calculation of biomass concentration (X , in g.kg^{-1}). The maximum specific growth rate was determined during exponential phase by fitting (Eq.9) with weighted least squares method.

$$X_t = X_0 \times e^{\mu_{max} \times t} \quad (9)$$

With X_t the biomass concentration at t time (g.kg^{-1}), X_0 the initial biomass concentration (g.kg^{-1}), μ_{max} maximum the specific growth rate (h^{-1}) and t the considered time for which the batch fermentation had been occurring (h).

344 *Glucose concentration analyses*

345 Glucose concentration was measured by high performance liquid chromatography (HPLC)
 346 from Waters Corporation (Milford, Massachusetts, the United States). Separation was carried
 347 out using a Varian Metacarb87P column 300 x 7.8 mm (Agilent Technologies, Santa Clara,
 348 California, the United States), at 31 bar and 80°C. Mobile phase was composed of ultrapure
 349 water with a flow rate of 0.4 mL.min⁻¹. Detection was achieved with a refractive index
 350 detector (Waters 2414) and glucose concentration (g.L⁻¹) was quantified using a range of
 351 calibration solutions.

352 *Staining and microscopy analyses*

353 Samples were diluted in 50 mmol.L⁻¹ phosphate-citrate buffer (pH 4.8) to reach a final
 354 biomass concentration of 2 to 5 g.kg⁻¹ (Hardy et al. 2016). They were stained at a ratio 1:4
 355 (v:v) with a commercial lactophenol-blue solution (Merck, Darmstadt, Germany) that was
 356 half-diluted with a solution of lactophenol-bleu without cotton blue and without phenol.
 357 Stained samples were fixed and sealed with nail varnish between a slide and a cover slip
 358 before microscopic observations. A bright field microscope AxioImager M2pCarl Zeiss AG
 359 (Oberkochen, Germany) bearing an N-Achroplan 20X objective (Carl Zeiss) was used. It was
 360 equipped with a motorized stage in X-Y-Z axis (steps: 0.1 µm, 0.1 µm and 25 nm), with a
 361 color camera 5 megapixels Axicam 105 Color through a video adapter 60N-C 2/3" 0.5x (Carl
 362 Zeiss). After white balance, normalization of light intensity and calibration, stacks of
 363 60 mosaics corresponding to a surface of 3.7 mm² and separated by 2 µm, were acquired
 364 (Hardy et al. 2016).

365 *Characterization of fungus morphology by image analysis*

366 Image analysis was carried out using a dedicated method described by Hardy et al. (2016).
 367 This method included an original extended depth-of-field approach, a specific segmentation
 368 and both skeleton and topological analyses. It led to the determination of 31 morphological

criteria from the acquisition of about one thousand fungal images per sample. Among these 31 criteria, four were retained as most relevant in relation to size and to damage due to fluid dynamic stress. For each fungal image, these four were the hyphal growth unit length (μm), the surface area (μm^2), the total length (μm) and the number of holes (nH). With respect to the latter, this advanced technique measures the three-dimensional clumped structure of each fungus. Thus the larger it is, the more folded it becomes as it is held between the glass plates used to help get clear images; and these holes relate to a combined effect of the size and extent of folding. Hardy et al. (2016) showed that when the fungi were exposed to extreme fluid dynamic stress levels, of the four criteria, the number of holes was the best measure of size, i. e. the lower the agitation intensity, the greater the number of holes. The value of nH recommended as a measure of size was the 90% quantile (q90) of the distribution of the number of holes per image.

3. RESULTS

Influence of bench scale stirring conditions on T. reesei cultures

Initially, fermentations of *T. reesei* were conducted with the stirrer shown in Fig 1.c at the bench scale at two stirring rates (800 rpm and 1700 rpm) to generate strongly different agitation conditions, namely a tip speed (V_{tip}) of 3.4 and 7.1 m.s^{-1} , a specific power input (P/V) of 6.2 and 59.5 kW.m^{-3} and an energy dissipation circulation function considering the maximum specific energy dissipation rate near the impeller ($\text{EDCF}_{\text{E}_{\text{max}}}$) of 94.2 and 1920.7 $\text{kW.m}^{-3}.\text{s}^{-1}$. The impact of these different conditions on *T. reesei* growth kinetics, on fermentation broth viscosity and on the fungus morphology was determined. Fig. 2 shows the growth curves of *T. reesei* including all of the data for both the duplicate runs for each of the two stirring conditions. As can be seen, the data from the two runs cannot be separated and in both cases for biomass concentrations below 8.2 g. kg^{-1} , the exponential growth indicates that

there was no growth limitation related to substrate concentration. Similar data were obtained in that biomass range in all fermentations undertaken. At 800 rpm, the maximum specific growth rate was equal to $0.082 (\pm 0.003) \text{ h}^{-1}$ whereas at 1700 rpm it was $0.065 (\pm 0.004) \text{ h}^{-1}$, a 20 % reduction of μ_{max} .

The apparent viscosity over the whole shear rate range from samples taken during the exponential growth phase when using the centripetal turbine are shown in Fig 3. At 800 rpm, data are shown for a sample taken at the end of that phase (8.2 g/kg) and another a little earlier (5.3 g/kg). Also shown are data from another experiment with agitation at 1700 rpm at a biomass concentration of 7.4 g/kg. It can be seen that though there is a difference between the apparent viscosities associated with the two biomass concentrations, there is a much greater difference between those at different speeds with similar biomass concentrations, with the apparent viscosity being ~ 5 times lower at the higher stirrer speed across the whole shear rate range. For precise comparison showing the impact of agitator speed at a shear rate of 10 s^{-1} , η_a falls from $0.659 \pm 0.053 \text{ Pa.s}$ to $0.127 \pm 0.001 \text{ Pa.s}$.

The morphology of *T. reesei* is illustrated in Fig. 4 where at 800 rpm, the quantile value $q_{90_{\text{NH}}}$ is $14.3 (\pm 1.3)$ while at 1700 rpm, it is $3.5 (\pm 0.5)$, a diminution 75 % of the number of holes at high stirring rate. From these results, it is very clear that agitation speed affected the growth kinetic of *T. reesei*, leading to changes in the morphology of the fungus and in the apparent viscosity of the fermentation medium.

Correlations for the effect of stirring at the bench scale on culture parameters

As a second step, *T. reesei* cultures were carried out at lab-scale with all four of the impellers shown in Fig. 1, at four different stirring rates (800, 935, 1250 and 1700 rpm), giving V_{tip} values of 3.5, 3.9, 5.2 and 7.1 m.s^{-1} , six values for P/V (6.2, 8.4, 17.9, 23.7, 59.5 and 59.6 kW.m^{-3}) and six for $\text{EDCF}_{\text{E}_{\text{max}}}$ (94.2, 196.1, 521, 561.4, 829.3 and $1920.7 \text{ kW.m}^{-3}.\text{s}^{-1}$).

Based on the three mixing parameters (V_{tip} , P/V and $EDCF_{\epsilon_{max}}$) expressed as $\ln(X)$ as the independent variable and the three fermentation parameters (growth rate, apparent viscosity at 10 s^{-1} , and indicator of morphology $q90$), as the dependent variable (Y), correlations were developed of the form:

$$Y = a \times \ln(X) + b \quad (10)$$

where a and b were fitted constants based on a linear regression, and reported in Table 2. In Fig. 5, the fermentation parameters are maximum specific growth rate (μ_{max} , in h^{-1}), apparent viscosity at 10 s^{-1} after fitting the data with a Herschel-Bulkley model (η , in Pa.s) and the quantiles 90 of the number of holes ($q90$). The correlation coefficients (R^2) for each case are also shown, and it is seen to be the lowest when V_{tip} was used as the independent variable and the highest with $EDCF_{\epsilon_{max}}$ whatever the dependent variable under consideration. P/V emerges also as an interesting parameter, but its R^2 coefficients are systematically lower than $EDCF_{\epsilon_{max}}$ ones. However, the similarity between the P/V and $EDCF_{\epsilon_{max}}$ criteria is not surprising given the expression of ϵ_{max} (Eq. 6). The $3/4$ exponent on Po , not far from 1, makes the way the two variables change with agitation intensity somewhat similar. Furthermore, in general, flow numbers of impellers do not change as much as power numbers and that is also true here where Fl for the four impellers used only differs by a factor 2.6 between the two extremes, thus making the induced circulation times similar in value.

Scale up of culture parameters

With respect to the fermentation parameters in the preliminary and full run at the commercial scale, the specific growth rates were the same (0.12 h^{-1}). In both cases, the apparent viscosity was very high compared to the bench scale but, as explained earlier, in the preliminary run, the protocol for ensuring a like-for-like comparison with respect to biomass concentration

was not well established. As a result, the biomass concentration was ~ 15 % higher, giving an apparent viscosity ~ 25% higher. Such a non-linear relationship is typical for such suspensions (Hardy et al., 2015). Overall, the results from the two large scale runs are essentially the same and very different from the bench scale. However, only the apparent viscosity value obtained with the matching biomass concentration has been used in the quantitative comparison of the large scale data with the bench scale in the discussion below.

Image analysis was only conducted on the full run.

Growth rate, viscosity and fungus morphology from the full run are reported in Fig. 5. The relative error of the prediction of the large scale value from the correlations developed at bench scale are reported on Fig. 5 (as “error”) and in Table 2 (% of the measured value). On the other hand,, Table 3 reports the fitted parameters of the correlations in Eq.10 and R^2 when both bench and commercial scale experimental results are used for the fitting procedure. Finally, Table 3 also reports the relative error when the correlations, based on data from both scales, are used to predict the large scale characteristics. Growth rate, morphology (number of holes) and apparent viscosity are all higher at large scale than at bench scale, which shows that these parameters are strongly coupled to hydrodynamic conditions. The error based on the extrapolation of the V_{tip} correlation gave a noticeably higher error (error range from 34 % to 65 %) for all criteria. The fact that the tip speeds at all scales are quite similar strongly suggests that tip speed is not a good scale up parameter (as also found in the earlier, much more limited scale-up study of Jüsten et al. (1996)). On the other hand, the predictions based on P/V and $EDCF_{\epsilon_{max}}$ were much better (error range from 5.5 to 25.3 %) with those for the latter being less than the former except for morphological parameter $q_{90_{nH}}$ (25.3 % for $EDCF_{\epsilon_{max}}$, 16.5% for P/V). These errors following scale-up by $EDCF_{\epsilon_{max}}$ correlations are very satisfying given that the range of values at the laboratory scale, which are used to fit the correlations, were obtained at $EDCF_{\epsilon_{max}}$ values higher by a factor 100 than the value at the

industrial scale. In addition, as pointed out above, in every case, R^2 for the correlations of the bench scale data was greatest with $EDCF_{\epsilon_{\max}}$. This result remains valid when bench and large scale experiments are used, as reported in Table 3, which shows the greater precision of the $EDCF_{\epsilon_{\max}}$ criteria.

A statistical t-test analysis gives P-values, reported in Table 4, that reinforce the consistency of the correlations in Tables 2 and 3 based on $EDCF_{\epsilon_{\max}}$. $EDCF_{\epsilon_{\max}}$ always furnishes lower P ($< 0.4\%$). P-values associated with P/V are slightly higher excepted for q90 ($P=2.5\%$), whilst the correlations based on V_{tip} are not statistically significant ($P > 5\%$).

Variations coefficients have also been calculated, considering correlation parameters of Table 3. They represent the part of the experimental variability that is not explained by the linear regressions. Variation coefficients are between 5% and 52% depending on the variable of interest and the chosen input parameter. As expected, the highest variation coefficients are associated with V_{tip} correlations, whereas the lowest ones are associated with $EDCF$ correlations (variations coefficients between 5% and 27%). As a conclusion, it can be stated that the $EDCF$ correlations explain the major part (72% or more) of the experimental variability, with the rest being linked with experimental uncertainty, including differences of biomass concentrations between samples as reported in Fig. 3.

4. DISCUSSION

On the effect of stirring intensity and choice of impeller at the bench scale

The different stirring conditions (geometry of the impellers and stirring rates) used in this study allowed very different fluid dynamic stress levels to be obtained. These stresses have been characterized by three main parameters: V_{tip} , P/V and $EDCF_{\epsilon_{\max}}$. In the literature, the ranges of V_{tip} were limited to 0.9 to 2.7 $m.s^{-1}$ (Lejeune and Baron 1995; Malouf et al. 2013; Marten et al. 1996; Patel et al. 2009) whereas here a much higher range of 3.5 to 7.1 $m.s^{-1}$

was obtained, more typical of those found on the commercial scale. For the parameters P/V and $EDCF_{\text{max}}$, no information is available with respect to *T. reesei*. However, similar ranges of $EDCF$ and P/V were explored with other filamentous fungi. With *Penicillium chrysogenum* and *Aspergillus oryzae*, Amanullah et al. (2002) using the former organism reported $EDCF$ values based on the swept volume between 2 and 1000 $\text{kW.m}^{-3}.\text{s}^{-1}$ and with the latter, Jüsten et al. (1996) used values ranging from 2 to 2000 $\text{kW.m}^{-3}.\text{s}^{-1}$, both with P/V values from 0.5 and 10 kW.m^{-3} . In this study, higher P/V values were obtained of 6.2 to 59.5 kW.m^{-3} , in order to avoid any oxygen transfer limitation. In addition, $EDCF_{\text{max}}$ values from 94.2 to 1920.7 $\text{kW.m}^{-3}.\text{s}^{-1}$, (corresponding to an $EDCF$ (swept volume) of 244 to 4971 $\text{kW.m}^{-3}.\text{s}^{-1}$) extended the range used previously as a result of the relative small volume of liquid used here at the bench scale.

Historically, impellers have often been described as either ‘low shear’ or ‘high shear’, where the former have a low Po/FI ratios and the latter, high ratios (Oldshue, 1983); and that terminology is still in use today (Lightnin’, 2016), though its usefulness has been questioned (Nienow, 2016). These terms imply that ‘low shear’ impellers would damage filamentous organisms less than ‘high shear’ at similar specific power. However, Jüsten et al. (1996; 1998) found that the opposite, e.g. ‘high shear’ Rushton turbines caused less damage than ‘low shear’ hydrofoil impellers with respect to morphology and productivity. In two of the fermentations here using the ‘high shear’ 4-blade disc paddle ($Po = 12$; $FI = 1.6$) at 935 rpm and the ‘low shear’ profiled tri-blade Rayneri impeller ($Po = 0.6$; $FI = 0.87$) at 1700 rpm, P/V was approximately the same ($58 \pm 1.5 \text{ kW m}^{-3}$). However, the equivalent $EDCF_{\text{max}}$ values were 830 $\text{kW.m}^{-3}.\text{s}^{-1}$ and 1920 $\text{kW.m}^{-3}.\text{s}^{-1}$ respectively. Under these conditions, the viscosity was 0.128 ($\pm 0.003 \text{ Pa.s}$) with the Rayneri and 0.258 ($\pm 0.020 \text{ Pa.s}$) with the 4-blade disc paddle. In addition, the specific growth rates were 0.061 (± 0.002) h^{-1} and 0.070 (± 0.003) h^{-1} and the number of q90 number of holes were 25 (± 2.2) and 31.2 (± 2.5) respectively. Thus, all

the process parameters indicate more damage with the ‘low shear’ impeller than with the ‘high’ one.

Another way to consider the effect of impeller type on $EDCF_{\varepsilon_{\max}}$ is to rearrange Eq. 7 using Eq. 2, 4 and 6 to eliminate the impeller speed, N . In this way, $EDCF_{\varepsilon_{\max}}$ can be written as a function of (P/V) to give:

$$EDCF_{\varepsilon_{\max}} \propto (V / \rho)^{1/3} (P/V)^{4/3} D^{-5/3} (Fl / Po^{7/12}) \quad (11)$$

If, in addition, it is assumed that $V \propto D^3$,

$$EDCF_{\varepsilon_{\max}} \propto (P/V)^{4/3} D^{-2/3} (Fl / Po^{7/12}) \quad (12)$$

Thus, at one scale, at constant P/V and D , so called “low shear” impellers (high Fl/Po ratios) will have a higher $EDCF_{\varepsilon_{\max}}$ than “high shear” impellers and can therefore potentially induce more damage to the filamentous fungi, as was shown in this study.

Fluid dynamic stress affected the growth of T. reesei

Comparison of the results obtained with the different stress conditions at the bench scale showed that increasing levels negatively impacted the maximum specific growth rate of *T. reesei*. This result confirms the observation of Lejeune and Baron (1995) who also showed that an increase of agitation speed reduced the growth of *T. reesei*, as indicated by the increase of the lag phase. However, these results disagree with those obtained by other authors (Malouf et al. 2013; Marten et al. 1996; Patel et al. 2009) who observed a positive impact of high agitation intensity on growth of *T. reesei*. This difference can probably be explained by the presence of some oxygen transfer limitation during their cultures since

unlike in the present work, dO_2 was not controlled, so that the elevated agitation speed would have increased it. There may also have been issues with substrate limitation as discussed further below.

*Fluid dynamic stress affected the 'viscosity' of *T. reesei* fermentation broth*

The apparent viscosity of the fermentation broth was reduced by increasing the stress level. This result agrees with that of Hardy et al.(2016). However, Marten et al.(1996) observed an increased viscosity at higher agitation speed whilst Patel et al.(2009) found that agitation speed did not affect viscosity, except for the lowest agitation speed that led to a lower viscosity. These differences may be ascribed to the lower agitation intensities explored in the earlier studies but again are more probably due to the fact that, at the agitation rates used, oxygen limitations occurred in the work of Patel et al.(2009), which reduced the growth of the fungus. On the other hand, as pointed out by the authors themselves, substrate limitations took place in the work of Marten et al.(1996), which induces fungal fragmentation, which in turn causes a reduction of the viscosity, as observed by Henaut et al.(2013). To avoid these problems, in this work, all experiments were performed without carbon limitation, by using directly fermentable substrates (lactose as a carbon source instead of cellulose) and a constant dO_2 of 40 % by gas blending (as done in the earlier work of Amanullah et al., (2002)). These conditions permitted the impact of agitation conditions to be dissociated from the effect of substrate and oxygen limitations, whilst also achieving conditions that are desired at large scale.

*Fluid dynamic stress affected the morphology of *T. reesei**

The stress conditions modified the morphological parameters that characterized the fungus during the growth phase. Notably, a decrease of 75 % of the number of holes inside the fungus was measured when the stress was highest. As discussed above, in the image analysis technique used in this study (Hardy et al. 2016), the larger the structure, the higher number

of holes. Thus, this reduction in the number of holes clearly shows that, in this work, high stresses also induced a reduction of the size of *T. reesei* cellular structures. This result is in agreement with those of Patel et al.(2009), but here it was obtained in conditions that avoided carbon and oxygen limitations, thus being more clearly associated with the impact of the fluid dynamic stresses (as well as being related to the desired large scale operating conditions)

Use of the different stress criteria to predict T. reesei culture parameters at commercial scale from bench scale studies

Uniquely, in this study, *T. reesei* culture parameters were also measured at the commercial scale. Thus it was possible to relate the maximum specific growth rate, the apparent viscosity of the broth and the morphological characteristics of the fungus at this scale to those predicted by three different criteria reflecting the fluid dynamic stresses arising from agitation. However, the morphology of the fungus and the rheological properties of the fermentation broth also depend on biomass concentration, in addition to agitation intensity (Hardy et al. 2015; Malouf et al. 2013). So, in order to dissociate the effect of biomass from the effect of the different stress parameters the rheological property measurements were made over a narrow range of biomass concentrations (4 to 8 g.kg⁻¹). This approach was complementary to that implemented by Malouf et al.(2013) who proposed correlations between rheological and morphological parameters that directly integrated the biomass concentration.

By comparing the three measured fermentation parameters with the three criteria of fluid mechanical stress (agitation intensity) of tip speed, power input per volume or EDCF_{εmax}, this study has demonstrated that the EDCF_{εmax} criterion was the most suitable for predicting the growth of *T. reesei*, the apparent viscosity of the broth and the morphology of the fungus at the commercial scale. Considering the fungus morphology, this result is in agreement with those of Jüsten et al. (1996) who showed that the EDCF concept is better able to correlate

591 morphological parameters than the other two criteria at different scales. Also as found by
 592 Jüsten et al. (1998), the EDCF concept was the best fit to the fermentation productivity, here
 593 in terms of maximum specific growth rate and in the earlier study, penicillin production. In
 594 addition, to our knowledge, for the first time, it is also seen that the apparent viscosity of the
 595 broth is best correlated and predicted by $EDCF_{\epsilon_{\max}}$. It is particularly effective at
 596 demonstrating that even though the tip speed at the commercial scale is similar to those at the
 597 bench scale, the apparent viscosity is much higher, just as the $EDCF_{\epsilon_{\max}}$ function predicts.
 598 The interconnections between all these variables can be explained by the fact that they are all
 599 dependent on the operating conditions (Quintanilla et al. 2015). The good result obtained
 600 with $EDCF_{\epsilon_{\max}}$ as independent variable is due to the integration of more phenomena than the
 601 other representations of fluid dynamic stress. Notably, as introduced by Smith et al. (1990)
 602 and Jüsten et al. (1996), it includes the notion of passage frequency of the fungi through the
 603 high energy dissipation region near the impeller, coupled with the maximum local specific
 604 energy dissipation rate in that region, both of which are important factors in determining the
 605 fluid mechanical stress ‘perceived’ by the fungus in the bioreactor. According to
 606 Stocks (2013), these two phenomena (frequency and intensity) may change in an opposite
 607 way during scale-up: frequency decreases at large scale, whereas fluid dynamic stress if
 608 defined by tip speed generally increases. This work clearly shows that V_{tip} is not an
 609 appropriate measure of stress. On the other hand, whilst the P/V parameter is proportional to
 610 the maximum specific energy dissipation rate, ϵ_{\max} , the allowance for the frequency of
 611 circulation through that region is found to improve the predictability.

612 The relative accuracy of the three different methods of predicting the three large scale
 613 fermentation parameters can be seen in Fig 5. Using $EDCF_{\epsilon_{\max}}$ as the independent variable to
 614 predict the viscosity of the fermented medium and the maximum specific growth rate of
 615 *T. reesei* at commercial scale led to error values lower than 5%, and 15% respectively,

whereas the error reached 25 % for the morphological criterion. Considering this information, the predictions of the viscosity and the specific growth rate seemed good, thus validating the use of $EDCF_{\epsilon_{\max}}$ as the best extrapolation factor for *T. reesei* cultures. The higher error in assessing the morphology of the fungus could be explained by the fact that there are many morphological criteria that could be used as explained by Hardy et al. (2016). Thus, those, which are best at bench scale as found here and in earlier work, may not be the best when extended to the commercial scale. Nevertheless, the trend is certainly correct.

5. CONCLUSIONS AND PERSPECTIVES

During *Trichoderma reesei* batch cultures at the bench and commercial scale, increasing fluid dynamic stress under conditions of controlled dO_2 and without nutrient limitation, has been shown to lower the apparent viscosity of the broth and the maximum specific growth rate and reduced the size of the fungus (reduced the number of holes as measured by image analysis). Three criteria (V_{tip} , P/V and $EDCF_{\epsilon_{\max}}$) were considered as measures of this stress and were correlated with the fermentation parameters measured at the bench scale. It was found that the $EDCF_{\epsilon_{\max}}$ function gave the best fit. These correlations were then used to predict the same parameters in a commercial scale bioreactor. This extrapolation showed again that $EDCF_{\epsilon_{\max}}$ was the best parameter to predict these variables, whilst the use of V_{tip} was extremely inaccurate. However, to draw out the difference in prediction performance between P/V and $EDCF_{\epsilon_{\max}}$, it is interesting to data fit Eq. 10 to the data from the runs at both scales. Again, it can be seen that the fit (Table 3) with the $EDCF_{\epsilon_{\max}}$ is the best in each case, giving further support to its use for predicting performance across the scales as well as the impact of different impellers.

Overall, this work has demonstrated that it was possible to make a scientifically based scale-up to commercial scale in relation to fluid dynamic stresses from scale-down experiments

640 done at the bench. In the future, these correlations should be improved by taking account the
641 effect of biomass concentration or by expanding the range of $EDCF_{\epsilon_{\max}}$ values used to reach
642 lower values. In addition, as the industrial strain used in this work exhibited an unusual
643 morphology, it would be interesting to expand this study by considering a well-known strain
644 such as *T. reesei* RUT-C30, to facilitate the comparison with previous works. Finally, it is
645 planned to use the correlations and approach established in this work to the production of
646 cellulases.

647 **ACKNOWLEDGMENTS**

648 The authors acknowledge the Agence de l'Environnement et de la Maîtrise de l'Energie
649 (ADEME, Angers, France) for financial support of PhD of Nicolas Hardy and Dr. Claudio
650 Pereira Da Fonte for Computational fluid dynamics characterization of the paddle impeller
651 (Power number, flow number).

652

653 NOMENCLATURE

654	a, b	Fitted constants in Eq. 10
655	D	Impeller diameter (m)
656	dO ₂	dissolved oxygen concentration (% from saturation value at ambient pressure)
657	EDCF	Energy dissipation/circulation function (W.m ⁻³ .s ⁻¹)
658	EDCF _{εmax}	EDCF considering the maximum specific energy dissipation rate (W.m ⁻³ .s ⁻¹)
659	Fl	Flow number of the impeller
660	K _{HB}	consistency index (Pa.s ⁿ)
661	N	Rotation speed (s ⁻¹)
662	n	flow behaviour index (-)
663	nH	number of holes in a fungal image
664	Po	Power number of the impeller
665	P	Power draw (W)
666	q90	90 % quantile in the distribution of nH in the images analysed <i>t</i> time (h)
667	<i>t_c</i>	Circulation time (s ⁻¹)
668	<i>t_m</i>	Mixing time (s ⁻¹)
669	R ²	Correlation coefficient
670	V	Volume of broth (m ³)
671	V _{tip}	Impeller tip speed (m.s ⁻¹)
672	VVM	Aeration of the broth (in normal Volume of air per Volume of liquid per minute)
673	W	Impeller blade width (see Table 1) (m)
674	X	Biomass concentration (g.kg ⁻¹); and independent variable in Eq. 10.
675	Y	Dependent variable in Eq. 10.
676	ε _{max}	Maximum local specific energy dissipation rate (W.m ⁻³)
677	μ _{max}	Maximum specific growth rate (h ⁻¹)

678 η_a Apparent viscosity (Pa.s)

679 ρ Density (kg.m^{-3})

680 $\dot{\gamma}$ Shear rate (s^{-1})

681 τ_{HB} Yield stress (Pa)

682 REFERENCES

683 Amanullah, A., Christensen, L.H., Hansen, K., Nienow, A.W., Thomas, C.R., 2002.
684 Dependence of morphology on agitation intensity in fed-batch cultures of *Aspergillus oryzae*
685 and its implications for recombinant protein production. *Biotech. Bioeng.* 77(7), 815-826.

686 Amanullah, A., Buckland, B.C., Nienow, A.W., 2004. Mixing in the Fermentation and Cell
687 Culture Industries. In: Paul, L.E., Atiemo-Obeng, A.V., Kresta, M.S. (Eds.). *Handbook of*
688 *Industrial Mixing*, John Wiley & Sons, Inc., Hoboken, pp. 1071–1170.

689 Amanullah, A., Jüsten, P., Davies, A., Paul, G.C., Nienow, A.W., Thomas, C.R., 2000.
690 Agitation induced mycelial fragmentation of *Aspergillus oryzae* and *Penicillium*
691 *chrysogenum*. *Biochem. Eng. J.* 5(2), 109–114.

692 Ayrinhac, C., Margeot, A., Ferreira, N.L., Chaabane, F.B., Monot, F., Ravot, G., Sonet, J.M.,
693 Fourage, L., 2011. Improved saccharification of wheat straw for biofuel production using an
694 engineered secretome of *Trichoderma reesei*. *Org. Proc. Res. and Dev.* 15(1), 275–278.

695 Bailey, J.E., Ollis, D.F., 1986. *Biochemical engineering fundamentals*, McGraw-Hill, New
696 York.

697 Bischof, R.H., Ramoni, J., Seiboth, B., 2016. Cellulases and beyond: The first 70 years of the
698 enzyme producer *Trichoderma reesei*. *Microbial Cell Factories*, 15(1), doi: 10.1186/s12934-
699 016-0507-6.

700 Cooke, M., Middleton, J.C., Bush, J.R., 1988. Mixing and mass transfer in filamentous
 701 fermentations. In: Proc. 2nd Int. Conf. on Bioreactor Fluid Dynamics, King, R. (Eds),
 702 Elsevier Applied Sciences, Elsevier, New York, pp 37 – 64.

703 Durand, H., Clanet, M., Tiraby, G., 1988. Genetic improvement of *Trichoderma reesei* for
 704 large scale cellulase production. *Enz. Microb. Tech.* 10(6), 341–346.

705 Elson, T.P., Cheesman, D.J., Nienow, A.W., 1986. X-Ray studies of cavern sizes and mixing
 706 performance with fluids possessing a yield stress. *Chem. Eng. Sci.* 41(10), 2555–2562.

707 Gabelle, J.C., Jourdier, E., Licht, R.B., Ben Chaabane, F., Henaut, I., Morchain, J., Augier,
 708 F., 2012. Impact of rheology on the mass transfer coefficient during the growth phase of
 709 *Trichoderma reesei* in stirred bioreactors. *Chem. Eng. Sci.* 75, 408–417.

710 Gabriele, A., Nienow, A.W., Simmons, M.J.H., 2009. Use of angle resolved PIV to estimate
 711 local specific energy dissipation rates for up- and down-pumping pitched blade agitators in a
 712 stirred tank. *Chem. Eng. Sci.* 64(1), 126–143.

713 Grenville, R.K., Brown, D., 2012. A method for comparing impellers' generation of
 714 turbulence and flow. MIXING XXIII conference, Mayan Riviera, Mexico, unpublished work.

715 Gusakov, A.V., 2011. Alternatives to *Trichoderma reesei* in biofuel production. *Trends in*
 716 *Biotech.*, 29(9), 419–425.

717 Hardy, N., Henaut, I., Augier, F., Béal, C., Ben Chaabane, F., 2015. Rheology of filamentous
 718 fungi: a tool for the comprehension of 2G-bioethanol production. *Rhéologie*, 27, 43–48.

719 Hardy, N., Moreaud, M., Guillaume, D., Augier, F., Nienow, A.W., Béal, C., Ben Chaabane,
 720 F., 2016. Advanced digital image analysis method dedicated to the characterisation of the
 721 morphology of filamentous fungus. *J. Microscopy*, accepted paper, doi: 10.1111/jmi.12523.

722 Henaut, I., Ben Chaabane, F., Lopes Ferreira, N., Augier, F., 2013. Experimental guidelines
 723 to optimize two crucial steps of lignocellulosic bioethanol production. *Journal of Sustainable*
 724 *Energy Engineering.* 1(4), 311–321.

- 725 Jüsten, P., Paul, G.C., Nienow, A.W., Thomas, C.R., 1996. Dependence of mycelial
726 morphology on impeller type and agitation intensity. *Biotech. Bioeng.* 52(6), 672–684.
- 727 Jüsten, P., Paul, G.C., Nienow, A.W., Thomas, C.R., 1998. Dependence of *Penicillium*
728 *chrysogenum* growth, morphology, vacuolation, and productivity in fed-batch fermentations
729 on impeller type and agitation intensity, *Biotech. Bioeng.* 59, 762–775.
- 730 Kolmogorov, A.N., Dissipation of Energy in the Locally Isotropic Turbulence, 1941. In:
731 *Proceedings: Mathematical and Physical Sciences*, 434, 1890, Turbulence and Stochastic
732 *Process: Kolmogorov's Ideas 50 Years On*, 1991, pp. 15-17.
- 733 Lejeune, R., Baron, G.V., 1995. Effect of agitation on growth and enzyme production of
734 *Trichoderma reesei* in batch fermentation. *Applied Microbio. Biotech.* 43(2), 249–258.
- 735 Lightnin Documentation, 2016. [http://www.spxflow.com/en/assets/pdf/B-](http://www.spxflow.com/en/assets/pdf/B-937%20LIGHTNIN%20General%20Brochure%20US.5.20.14_tcm11-9420.pdf)
736 [937%20LIGHTNIN%20General%20Brochure%20US.5.20.14_tcm11-9420.pdf](http://www.spxflow.com/en/assets/pdf/B-937%20LIGHTNIN%20General%20Brochure%20US.5.20.14_tcm11-9420.pdf), accessed 9th
737 December, 2016.
- 738 Malouf, P., Patel, N., Rodrigue, D., Thibault, J., 2013. Relationship between morphology and
739 rheology during *Trichoderma reesei* RUT-30 fermentation. *Rheology: Theory, Properties and*
740 *Practical Applications.*, (phD thesis), Ottawa University.
- 741 Marten, M., Velkovska, S., Khan, S.A., Ollis, D.F., 1996. Rheological, mass transfer, and
742 mixing characterization of cellulase - producing *Trichoderma reesei* suspensions. *Biotech.*
743 *Progress.* 12(5), 602–611.
- 744 Metzner, A.B., Otto, R.E., 1957. Agitation of non-Newtonian fluids. *AIChE J.* 3(1), 3–10.
- 745 Mezger, T., 2014. *The rheology handbook: For users of rotational and oscillatory rheometers.*
746 Vincentz Network Gmbh & Co KG . Hannover.
- 747 Nienow, A.W., 1998. Hydrodynamics of stirred bioreactors. *App. Mech. Rev.* 51(1), 3–32.
- 748 Nienow, A.W., 2016. Stirred, not shaken; flow and shear impellers revisited. *ICHEME Fluid*
749 *Mixing Processes Special Interest Group, Webinar Series: Fundamentals Webinar 1*, April,

- 2016.
- Oldshue, J.Y., 1966. Fermentation mixing scale-up techniques. *Biotech. and Bioeng.* 8(1), 3-24.
- Oldshue, J.Y., 1983. *Fluid Mixing Technology*, McGraw Hill, New York.
- Patel, N., Choy, V., Malouf, P., Thibault, J., 2009. Growth of *Trichoderma reesei* RUT C-30 in stirred tank and reciprocating plate bioreactors. *Process Biochem.* 44(10), 1164–1171.
- Percival Zhang, Y.H., Himmel, M.E., Mielenz, J.R., 2006. Outlook for cellulase improvement: Screening and selection strategies. *Biotech. Adv.* 24(5), 452–481.
- Pourquié, J., Warzywoda, M., Chevron, F., Thery, D., Lonchamp, D., Vandecasteele, J.P., 1988. Scale up of cellulase production and utilization. In *FEMS Symposium n°43: Biochemistry and Genetics of Cellulose Degradation*. Aubert J-P, Beguin P, Millet J. (Eds), Academic Press, London, pp 71–86.
- Quintanilla, D., Hagemann, T., Hansen, K., Gernaey, K.V., 2015. Fungal morphology in industrial enzyme production modelling and monitoring. *Adv. Biochem. Eng./Biotechn.* 149, 29–54.
- Riley, G.L., Tucker, K.G., Paul, G.C., Thomas, C.R., 2000. Effect of biomass concentration and mycelial morphology on fermentation broth rheology. *Biotech. Bioeng.* 68(2), 160-172.
- Sánchez Pérez, J.A., Rodríguez Porcel, E.M., Casas López, J.L., Fernández Sevilla, J.M., Chisti, Y., 2006. Shear rate in stirred tank and bubble column bioreactors. *Chem. Eng. J.* 124(1-3), 1–5.
- Serrano-Carreón, L., Galindo, E., Rocha-Valadéz, J.A., Holguín-Salas, A., Corkidi, G., 2015. Hydrodynamics, fungal physiology, and morphology. *Adv. Biochem. Eng./Biotech.* 149, 55–90.
- Simbolotti, G., 2007. *IEA Energy Technology Essentials: Biofuel Production*. Paris.

774 Singh, V., Hensler, W., Fuchs, R., Constantinides, R., 1986. On line determination of mixing
775 parameters in fermenters using pH transients, Proc. Intl. Conf. Bioreactor Fluid Dynamics,
776 231.

777 Smith, J.J., Lilly, M.D., Fox, R.I, 1990. The effect of agitation on the morphology and
778 penicillin production of *Penicillium chrysogenum*. Biotech. Bioeng. 35(10), 1011–1023.

779 Stocks, S.M., 2013. Industrial enzyme production for the food and beverage industries:
780 Process scale up and scale down. Microbial Production of Food Ingredients, Enzymes and
781 Nutraceuticals, <http://dx.doi.org/10.1533/9780857093547.1.144>.

782 van't Riet, K., Tramper, J., 1991. Basic bioreactor design. New York. In: M. Dekker.

783 Wang, D.I.C., Cooney, C.L., Demain, A.L., 1979. Fermentation and Enzyme Technology.
784 New York, J.Wiley & Sons, 374.

785 Wucherpennig, T., Kiep, K.A., Driouch, H., Wittmann, C., Krull, R., 2010. Morphology and
786 Rheology in Filamentous Cultivations. Adv. Applied Microbiology, 72, 89-136.

787

788

789

790

791 **Table Captions**

792

793 Table 1: Mixing and geometric characteristics of the impellers used in the study. ⁽¹⁾ Data from
794 VMI the Mixing Company Rayneri (Montaigu, France); ⁽²⁾ Data obtained by Computational
795 Fluid Dynamics at IFPEN (Rueil-Malmaison, France) with the software ANSYS CFD from
796 Ansys (Cecil Township, Pennsylvania, U.S.A.) using the Moving Reference Frame method.

797

798 Table 2: Correlation coefficients (Eq.10) - Fit at Bench scale only

799

800 Table 3: Correlation coefficients (Eq.10) - Fit at Bench and Commercial scale

801

802 Table 4: P-values corresponding to t-test of Eq.10, based on correlation parameters of Tables
803 2 and 3.

804

Figure Captions

Fig. 1. Pictures of the impellers used in the study, with associated symbols. (a) Propeller; (b) Profiled triblade; (c) Centripetal turbine; (d) 4-blade disc paddle; The scale bar in the upper-left corner represents 10 cm.

Fig. 2. Growth curves characterizing duplicate batch fermentations of *T. reesei* under two stirring conditions with data from duplicate runs at each speed included. The centripetal turbine is used at a speed rate of 800 rpm (white) and 1700 rpm (black). Arrows point to time when samples were taken for apparent viscosity and image analysis measurements.

Fig. 3. Dynamic apparent viscosity versus shear rate for culture samples of *T. reesei* fungi. Samples were collected during exponential growth phase at 800 rpm using the centripetal turbine, 5.3g/kg (white circles) and 8.2g/kg of biomass (white triangles), and at 1700 rpm and 7.4g/kg of biomass (black circles). Duplicates with two cycles per sample are presented for each condition.

Fig. 4. Representative pictures of *T. reesei* morphology after cultures conducted at 800 rpm (A and B) and 1700 rpm (C and D). The images are composed of mosaics of 16 subimages, with a size of 10098 per 7538 pixels. They were obtained before segmentation (A and C) or after segmentation (B and D). Holes are shown in red in the segmented images. Width of images is 2 mm.

Fig. 5. Comparison of growth, rheological and morphological parameters obtained from predictions based on three fluid dynamic stress criteria. V_{tip} : tip speed (in $m.s^{-1}$); P/V : power input per volume (in $kW.m^{-3}$); $EDCF(\epsilon_{max})$: EDCF considering the maximum specific energy dissipation (in $kW.m^{-3}.s^{-1}$). Marker's sizes are proportional to biomass concentrations. Propeller (square); Profiled triblade (inverted triangle); Centripetal turbine (circle); 4-blade disc paddle (star); Commercial scale (black cross). 800 rpm (white); 935 rpm (light-grey); 1250 rpm (dark-grey); 1700 rpm (black). R^2 are the correlation coefficients for the linear

models in logarithmic scale; errors represent the difference (in %) between predictions of a parameter and its measurement at commercial scale.

Figures

Figure 1

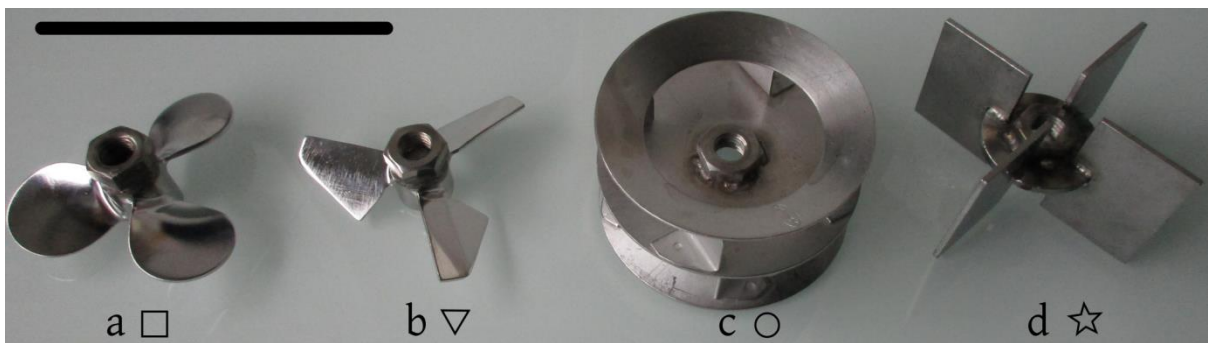


Fig. 1. Pictures of the impellers used in the study, with associated symbols. (a) Propeller; (b) Profiled triblade; (c) Centripetal turbine; (d) 4-blade disc paddle; The scale bar in the upper-left corner represents 10 cm.

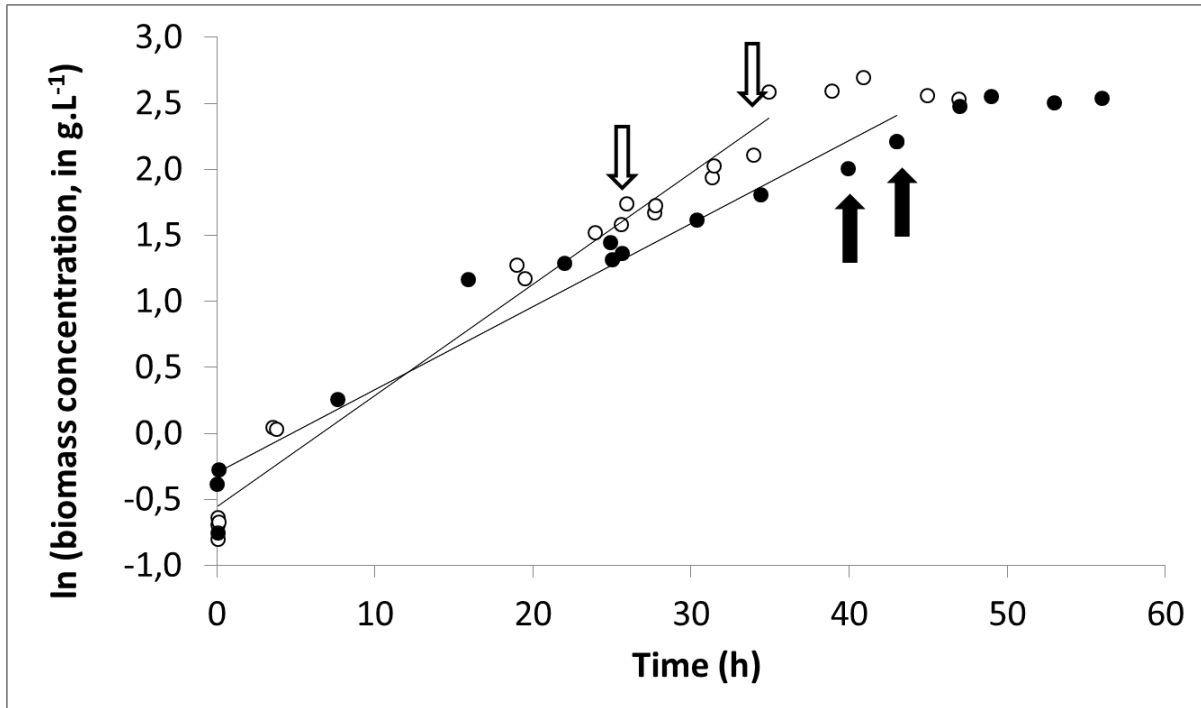


Fig. 2. Growth curves characterizing duplicate batch fermentations of *T. reesei* under two stirring conditions with data from duplicate runs at each speed included.

The centripetal turbine is used at a speed rate of 800 rpm (white) and 1700 rpm (black).

Arrows point to time when samples were taken for apparent viscosity and image analysis measurements.

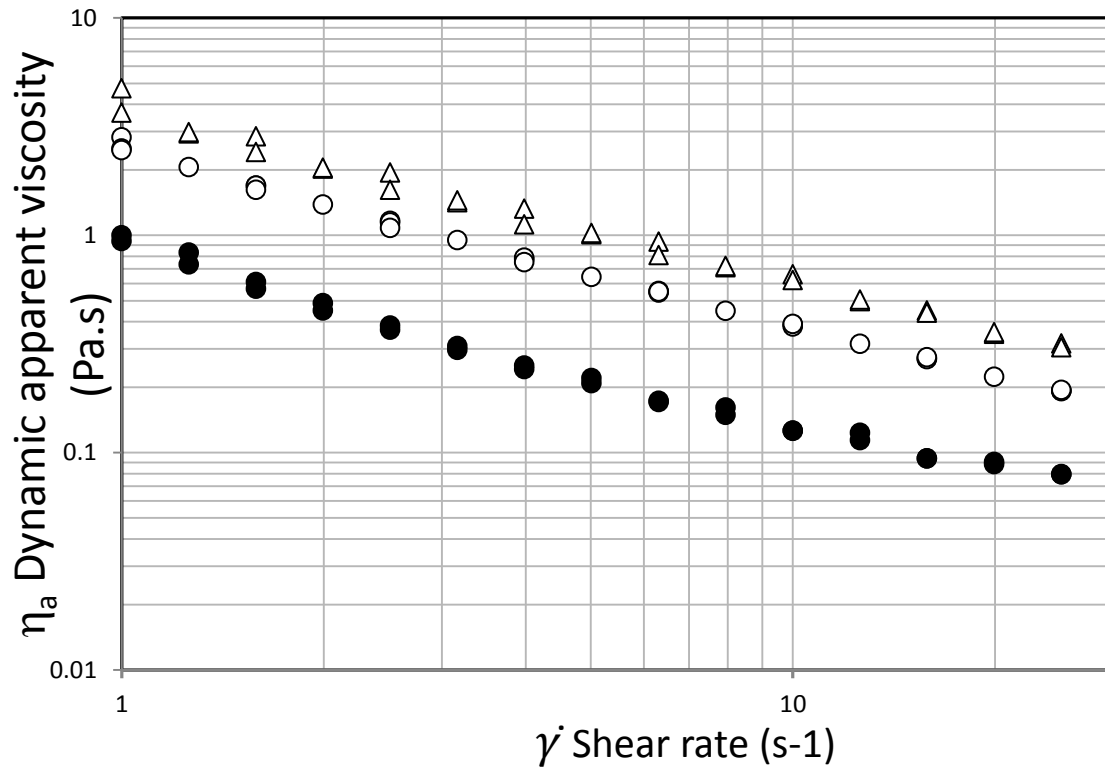


Fig. 3. Dynamic apparent viscosity versus shear rate for culture samples of *T. reesei* fungi. Samples were collected during exponential growth phase at 800 rpm using the centripetal turbine, 5.3g/kg (white circles) and 8.2g/kg of biomass (white triangles), and at 1700 rpm and 7.4g/kg of biomass (black circles). Duplicates with two cycles per sample are presented for each condition.

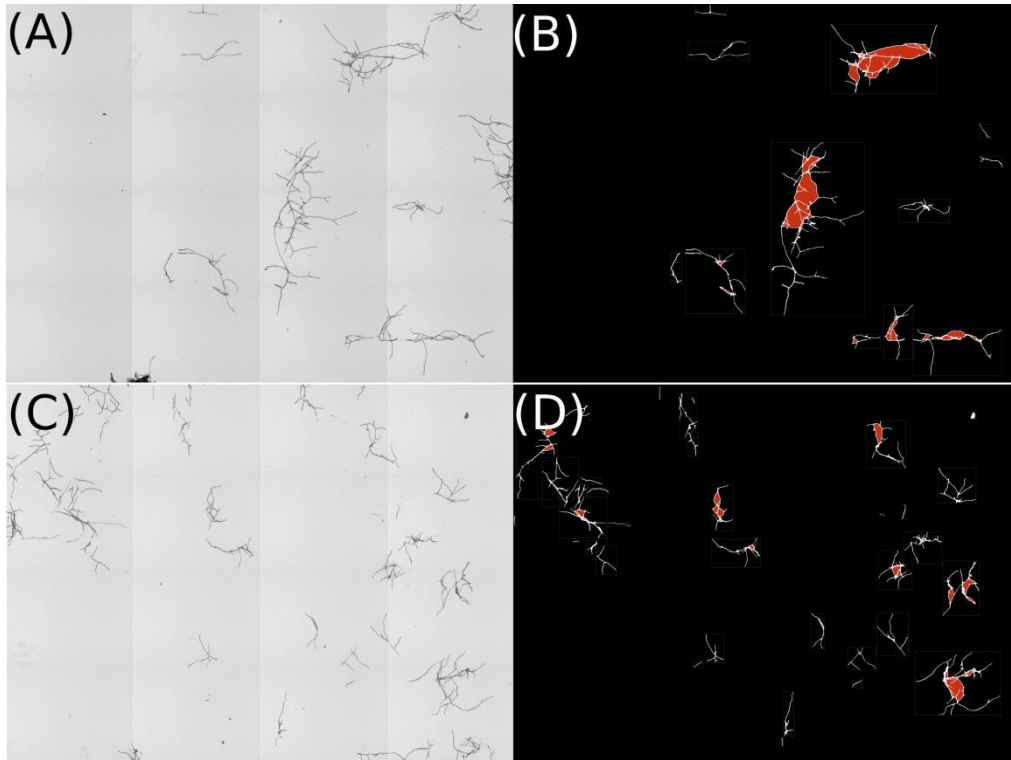
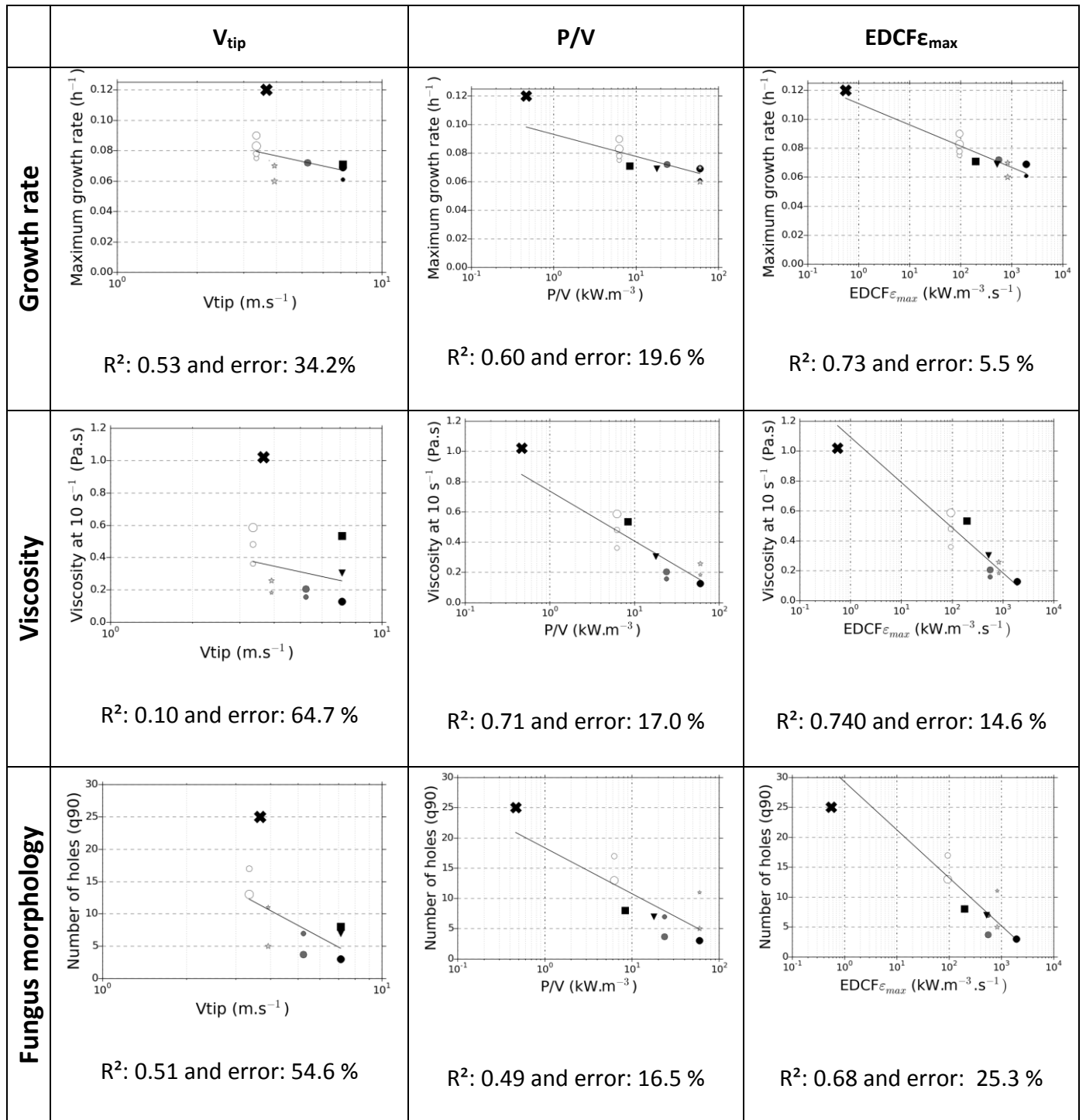


Fig. 4. Representative pictures of *T. reesei* morphology after cultures conducted at 800 rpm (A and B) and 1700 rpm (C and D).

The images are composed of mosaics of 16 subimages, with a size of 10098 per 7538 pixels. They were obtained before segmentation (A and C) or after segmentation (B and D). Holes are shown in red in the segmented images.

Width of images is 2 mm.

864



865

866

Fig. 5. Comparison of growth, rheological and morphological parameters obtained from predictions based on three fluid dynamic stress criteria.

867

868

V_{tip} : tip speed (in $m.s^{-1}$); P/V : power input per volume (in $kW.m^{-3}$); $EDCF_{\epsilon_{max}}$: EDCF

869

considering the maximum specific energy dissipation (in $kW.m^{-3}.s^{-1}$).

870 *Marker's sizes are proportional to biomass concentrations.*

871 *Propeller (square); Profiled triblade (inverted triangle); Centripetal turbine (circle); 4-*

872 *blade disc paddle (star); Commercial scale (black cross).*

873 *800 rpm (white); 935 rpm (light-grey); 1250 rpm (dark-grey); 1700 rpm (black).*

874 *R² are the correlation coefficients for the linear models in logarithmic scale; errors*

875 *represent the difference (in %) between predictions of a parameter and its measurement at*

876 *commercial scale.*

877

878

879